

**Fractal Dimension Assessment of
Dibenz[a,l]pyrene Oral Carcinogenesis**

BY

YAJUR PARIKH

B.S., University of Illinois at Urbana-Champaign, 2003

THESIS

Submitted as partial fulfillment of the requirements
for the degree of Master of Science in Bioengineering
in the Graduate College of the
University of Illinois at Chicago, 2014

Chicago, Illinois

Defense Committee:

Joel Schwartz, Chair and Advisor, Oral Medicine and Diagnostics
Thomas Royston
Sara Gordon, Oral Medicine and Diagnostics

ACKNOWLEDGEMENTS

I would like to thank my thesis committee for the crucial roles that each of them played to help me accomplish my goal of completing and defending my thesis. Thank you to Dr. Joel Schwartz for thinking of the idea that became the basis for my research and for the original study he performed at UIC that provided much of the necessary data. Thank you to Dr. Thomas Royston for connecting me with Dr. Schwartz and for being available on short notice to review my thesis and serve on my committee. Thank you to Dr. Sara Gordon for her many hours spent providing me with revisions for my thesis and for helping me structure it more clearly and coherently.

I would also like to thank Hajwa Kim from the UIC Center for Clinical and Translational Science for helping me to understand the necessary biostatistical analysis methods for my research.

TABLE OF CONTENTS

<u>CHAPTER</u>	<u>PAGE</u>
SUMMARY	viii
1. INTRODUCTION	1
1.1 Background of OSCC	1
1.1.1 Definition	1
1.1.2 Epidemiology and risk factors	2
1.1.3 Pathogenesis	2
1.1.4 Clinical features	3
1.1.4.1 Premalignant diseases	3
1.1.4.2 OSCC	4
1.1.5 Prognosis and treatment	4
1.1.6 Diagnosis	5
1.1.6.1 Issues with histopathologic diagnosis	5
1.2 Fractal analysis background	6
1.2.1 Fractal history	6
1.2.2 Fractal uses for pathology	8
1.2.3 New technologies for fractal analysis	8
1.3 Infiltrate analysis background	9
1.4 Clustering background	9
2. HYPOTHESIS	11
3. METHODS	12
3.1 Hamster oral carcinogenesis studies	12
3.2 Slide analysis	14
3.2.1 Slide conversion to digital format	14
3.2.2 Fractal analysis procedure	15
3.2.2.1 Simple box count	16
3.2.2.2 Subscans	18
3.2.2.3 Full tissue scans	19
3.2.3 Inflammatory infiltrate analysis	20
3.2.4 Classifying by pattern of tumor invasion	21
3.2.5 Statistical data analysis	23
3.2.6 Advanced statistical data analysis	24
3.2.6.1 Two-step cluster analysis and ANOVA	25
3.2.6.2 Receiver operating characteristic	26

TABLE OF CONTENTS (continued)

<u>CHAPTER</u>	<u>PAGE</u>
4. RESULTS	27
4.1 Hamster carcinogenesis results	27
4.2 Fractal dimension and lacunarity results	27
4.3 Inflammatory infiltrate results	33
4.4 Advanced analysis results	37
5. DISCUSSION	41
5.1 Hamster model and fractal-based analysis	41
5.2 Uses of advanced statistics	44
5.3 Future aims	46
6. CONCLUSIONS	47
CITED LITERATURE	48
APPENDIX	51
VITA	52

LIST OF TABLES

<u>TABLE</u>	<u>PAGE</u>
1. Histopathology for dysplasia following exposure to BP, DBP (tongue)	13
2. Incidence of tumor formation by treatment	13
3. Box count fractal dimension and lacunarity classified by pattern of tumor invasion	28
4. Inflammatory infiltrate statistics classified by pattern of tumor invasion ...	34
5. Fractal Dimension ROC Curve Results	39
6. Lacunarity ROC Curve Results	39

LIST OF FIGURES

<u>FIGURE</u>	<u>PAGE</u>
1. Change in oral mucosa with application of dibenz[a,l]pyrene	14
2. Conversion process of digital slides through steps	15
3. Patterns of tumor invasion based on epithelial structure	22
4. Simple box count FD grouped by POI	29
5. Simple box count lacunarity grouped by POI	30
6. Box count fractal dimension and lacunarity scatter plot grouped by POI ...	32
7. Inflammatory infiltrate total area grouped by POI	35
8. Inflammatory infiltrate area fraction grouped by POI	35
9. Inflammatory infiltrate total area and area fraction scatter plot grouped by POI	37

FREQUENTLY USED ABBREVIATIONS

B[a]P	Benzo[a]pyrene
DBP	Dibenz[a,l]pyrene
FD	Fractal dimension
HNSCC	Head and neck squamous cell carcinoma
HPV	Human papillomavirus
OSCC	Oral squamous cell carcinoma
PAH	Polycyclic aromatic hydrocarbons
POI	Pattern of tumor invasion
ROI	Region of interest

SUMMARY

Oropharyngeal and oral squamous cell carcinoma (OSCC) is diagnosed in approximately 270,000 patients worldwide per year, leading to 100,000 to 200,000 deaths in a typical year (Jemal, Bray et al. 2011). OSCC is linked to environmental carcinogens such as polycyclic aromatic hydrocarbons (PAH). Activities that can increase the risk of OSCC include the use of tobacco, alcohol, or betel nuts, and exposure to certain types of human papillomavirus (HPV).

Histopathologic diagnosis relies upon recognition of a change of pattern in tissue architecture. Pathologists may disagree on these diagnoses, which can have important consequences for patient treatment and prognosis (Saxen, Franssila et al. 1978, Presant, Russell et al. 1986). Diagnostic methods are needed to improve and enhance accuracy, especially to help distinguish between degrees of premalignant change, squamous carcinoma and aggressive subtypes of squamous cell carcinoma. One such method could be the use of conventional pathology-based criteria in combination with software that objectively measures specific changes in tissue patterns within biopsy specimens, reflecting changes in the biologic activity of epithelial cells as they interact with underlying mesenchymal tissues (Mani, Guo et al. 2008). We suggest that the use of pattern recognition algorithms found in publicly available software could improve histopathologic diagnostic accuracy. This approach will provide an objective, decision-oriented capability not currently available to pathologists for routine diagnosis. Our long-term goal is to improve prognosis and treatment outcomes for patients with head and neck squamous cell carcinomas (HNSCC).

In this study we develop a pattern recognition image approach based upon fractal dimension (FD) analysis in order to bolster histopathologic assessment and to better discriminate stages of dysplasia from OSCC. Compared to previous published studies, this project seeks to test the capability for FD analysis to assist with histopathologic diagnosis by evaluation of tissues from a controlled oral carcinogenesis model. Using a mathematical cluster approach, we validate the combination of enhanced FD determination, together with additional mathematical validation and histopathologic criteria that have already demonstrated prognostic capability for human tissues. Taken together, this is unique in the field of histopathology diagnostic tool development.

1. INTRODUCTION

1.1 Background of OSCC

The development of OSCC in humans involves hundreds of changes in normal epithelial cells as they transform toward a malignant state. Current and previous studies have generally addressed OSCC development using genetic, chemical and molecular biologic approaches. These studies characterize cellular growth among epithelial cell populations by exploring a variety of cell pathways, providing further insight into normal physiology and cell-to-cell interactions. These factors must be sufficiently identified and understood in order to improve treatment options and survivability prognosis for patients (Brandwein 2005). However, there is still not enough progress in terms of improving prognosis. Alternate paths of study that have not been as well explored include mathematical models to describe cell growth and potentially aid diagnosis.

1.1.1 Definition

Oral squamous cell carcinoma is defined as the uncontrolled growth of malignant epithelial cells in the epithelial layer of the oral cavity as well as the oropharynx, which includes the base of the tongue, tonsils, soft palate, and pharynx walls (Neville, Damm et al. 2009). Other oral cancers do occur, including adenocarcinomas, sarcomas and lymphomas, but OSCC accounts for 90% of all oral cancers (Park 2009).

1.1.2 Epidemiology and risk factors

As with most other cancers, the risk of OSCC is affected by a wide variety of factors, both intrinsic and extrinsic. In the vast majority of OSCC cases, several of these factors combine to produce a malignancy. One of the key extrinsic factors is exposure to tobacco smoke, as approximately 80% of U.S. patients with oral carcinoma are tobacco smokers, versus just 21% of the general U.S. population (Neville, Damm et al. 2009). This includes the use of cigarettes, cigars, or pipes. Related to this factor is the use of smokeless tobacco, including products such as snuff, snus, and chewing tobacco, which are placed in the mouth during use. Approximately 50% of oral cancers in smokeless tobacco users occur at the site in the mouth where the tobacco is placed (Neville, Damm et al. 2009).

In addition, excessive alcohol consumption can also contribute to the development of OSCC, in particular when combined with the use of tobacco, which can increase the risk of oral cancer in a patient by a factor of 15. Cirrhosis of the liver, a symptom of heavy alcohol consumption, can be found in 20% of male oral cancer patients, a rate twice that of the general population (Neville, Damm et al. 2009).

The presence of the human papillomavirus (HPV) is also a significant risk factor in the development of OSCC. This specifically includes HPV subtypes 16, 18, 31, and 33. HPV includes proteins such as E6 and E7, which actively degrade tumor suppressors including p53 and pRb (retinoblastoma protein). Genetic factors also play a key role in OSCC development. These include the deactivation or mutation of tumor

suppressor genes, including p53 and pRb as mentioned above, and genes such as p16 and E-cadherin (Neville, Damm et al. 2009)

1.1.3 Pathogenesis

The development of OSCC occurs over several stages. Cellular changes corresponding to the clinical findings can be categorized as premalignant to invasive. Premalignant changes range from very mild cellular atypia, through mild, moderate, and severe dysplasia, to carcinoma in situ. These categories of diagnosis are based upon the observation of progressively severe changes in cellular morphology, as well as the overall structure of the epithelium.

In dysplasia, changes are seen in the overall epithelial architecture and also in the morphology of individual cells. These changes include anaplasia; accumulation of keratin in basal or supra basal cells; an increase in nuclear and chromatin content resulting in an increase in the size of nuclei relative to the amount of cytoplasm; bizarre mitotic figures; and inappropriate chromosome segregation. Changes in overall epithelial architecture include loss of intercellular attachments; hyperkeratosis; hyperplasia, an increased number of keratinocytes per millimeter squared; expansion of rete pegs; and downward growth of epithelium without invasion.

As the disease progresses from dysplasia to outright malignancy, the epithelium begins to invade the underlying connective tissue. At this point, there is disintegration of the basement membrane that separates epithelium from the underlying tissues. Thus, diagnosis of squamous cell carcinoma is based on the presence, extension and

amplification of the above criteria, with breakdown of the basement membrane and a downward growth of transformed, proliferative basal cells that are increasingly variable in microscopic appearance. There is also an increasing infiltration of selective populations of immune effector suppressors,

1.1.4 Clinical features

OSCC develops slowly out of precursor dysplastic lesions. These are often red, white or a mixture of colors, and may have a rough or velvety surface. As the disease progresses, the lesion may become ulcerated and fixed to surrounding structures, and pain may develop.

1.1.4.1 Premalignant diseases

Early dysplasia often appears white (leukoplakia), red (erythroplakia) or mixed (erythroleukoplakia). Leukoplakia, erythroplakia and erythroleukoplakia are not always premalignant; some are reactive or may be other diseases. However, the proportion of cases that are dysplastic increases with lesions that are predominantly red.

Early stage thin leukoplakia appears as gray-white plaque, which is typically soft and flat. This may develop into thick or nodular leukoplakia, which develops increased irregularities and appears leathery in nature. Erythroplakia is more likely to signal dysplasia. More than half of all dysplastic lesions occur on the lateral and ventral tongue; about a quarter occur on the floor of the mouth (Neville, Damm et al. 2009).

Betel nut users may develop an unusual precancerous condition known as oral submucous fibrosis. This is characterized by mucosal rigidity and hyperplasia. The condition often develops dysplasia and invasive OSCC, in addition to a burning sensation and stiffness in the subepithelial tissues (Neville, Damm et al. 2009).

1.1.4.2 OSCC

The early growth phase of OSCC involves minimal pain to the patient, as the epithelial layer does not contain blood vessels or nerves. As OSCC develops, the lesion becomes exophytic with an irregular texture and an ulcerated surface (Neville, Damm et al. 2009). The tumor invades the connective tissue, where it may cause pain by invading nerve sheaths. It may also invade blood vessels and lymphatic channels, allowing it to metastasize to other sites.

1.1.5 Prognosis and treatment

Treatment of OSCC depends on the location and stage of the disease. Methods can include surgical excision, radiation therapy, or a combination of the two.

Oropharyngeal lesions are often treated with radiation, and may involve chemotherapy treatment with platinum-containing compounds, monoclonal antibodies, or small molecule inhibitors (Neville, Damm et al. 2009).

For intraoral carcinomas, especially ones which are deeply invasive or have metastasized in the lymph nodes, neck dissection may be performed, involving the removal of significant portions of fibrofatty tissues in the neck (Yuen, Wei et al. 1997).

Five-year survival rates for oral cancer depend heavily on tumor stage. The rates vary from 53% to 68% for intraoral carcinomas found and treated at Stage I or II, but fall significantly to just 27% for Stage IV tumors. A proper diagnosis is crucial to making sure the appropriate treatment is administered, and is one of the key goals of this project (Neville, Damm et al. 2009).

1.1.6 Diagnosis

Arriving at a histopathologic diagnosis for dysplasia or OSCC involves obtaining a tissue sample from the patient for biopsy. Ideally, these tissues should be taken from the most severely affected portions of the region. The biopsy is then evaluated by a pathologist using light microscopy. Samples of the affected tissue are taken, inserted into slides, and stained for viewing. A pathologist using light microscopy then evaluates the biopsy (Neville, Damm et al. 2009).

1.1.6.1 Issues with histopathologic diagnosis

A key issue with oral histopathologic diagnosis is inter-observer variability. Several studies have shown that a significant disagreement often exists between multiple pathologists diagnosing the same tissue sample. Using a more analytical method of diagnosis would provide a more objective result and could reduce the effects of clinician error (Abbey, Kaugars et al. 1995, Kujan, Khattab et al. 2007). Criterion-referenced classification schemes have been developed for a number of human neoplasms, and these partially overcome this problem by reducing, although not

eliminating inter-observer and even intra-observer variability. Such a histologic risk assessment for oral epithelial neoplasia was published by Brandwein-Gensler et al (Brandwein 2005) and is based on the lesion's worst pattern of invasion, the presence or absence of perineural invasion, and the degree of inflammatory response to the lesion.

The process of taking the tissue sample for biopsy is destructive to the surrounding tissue and is also subject to selection bias. If the surgeon does not sample the most aggressive portion of the lesion, or the biopsy is inadequate, under-diagnosis may occur.

1.2 Fractal analysis background

1.2.1 Fractal history

By the early 20th century, mathematicians had realized that irregular or fragmented shapes could not be properly understood through the use of existing measures of standard, known as Euclidean dimensions. Mathematicians of the period such as Cantor and Hausdorff realized that the dimension of an element need not be an integer. Instead, log functions could be used to determine a dimension D , which is separate from the Euclidean, topographic dimension denoted by D_T .

In 1967, Benoît Mandelbrot published his paper, "*How Long Is the Coast of Britain? Statistical Self-Similarity and Fractional Dimension*", which discussed a series of curves with a dimension between 1 and 2 (Mandelbrot 1967). In the paper, Mandelbrot discusses the paradox in which the measured length of a coastline depends

upon the scale of measurement. That is, a stretch of coastline measured with a yardstick would result in a shorter measured length than if a foot long ruler was used. The evidence showed that the length increases without limit as the measurement scale decreases towards zero. In this paper, the following law from Lewis Fry Richardson is used:

$$L(G) = MG^{1-D}$$

Equation 1

where M is a positive constant, D is a constant, the dimension, and $L(G)$ is the length of the shape's border (Mandelbrot 1967). This led Mandelbrot to prefer a method of measurement other than length, and to focus on *fractals*, a term he coined in 1975 to describe any set in which $D > D_T$ (Mandelbrot , Mandelbrot 1983).

A fractal has characteristics including: being a fine structure at small scales; having an irregularity that prevents it from being defined by Euclidean geometry; and especially that of being self-similar—that is, being composed in such a way that that the shape can be split into parts, each of which is approximately a reduced-size copy of the whole (Mandelbrot 1983). Fractal patterns can be found in fields as varied as music, miniature antennas, signal compression, weather, and economics (Hsü and Hsü 1990, Williams 1995, Gianvittorio and Rahmat-Samii 2002, Viswanath 2004).

Because fractal shapes tend to appear often in nature, a fractal-based analysis can be used to describe the geometry of natural features including astronomy, bacterial cultures, and plants. Fractal analysis has previously been used to analyze radiographic

and ultrasonic images of potentially cancerous tissue (Esgiar and Chakravorty , Kikuchi, Kozuma et al. 2002, Chang, Chen et al. 2004, Goutzanis, Papadogeorgakis et al. 2008).

1.2.2 Fractal uses for pathology

The use of fractal analysis specifically for histopathologic classification was first described in the late 1980s and early 1990s, and has allowed for new ways of observing and diagnosing tissue samples (Landini 1991, Cross and Cotton 1992, Sanders and Crocker 1993). This includes fractal dimension (FD) analysis of histology as a prognostic factor for cancer (DELIDES, PANAYIOTIDES et al. 2005). However, these studies have typically involved human tissue, which is subject to far more environmental factors and has a more complex carcinogenesis process than that of hamster tissue. In addition, images from sources such as ultrasound do not provide the cell-level of detail needed to study the process of carcinogenesis through various stages of dysplasia. The model and methods used in this study will allow for a more controlled environment of both test subjects and carcinogens.

1.2.3 New technologies for fractal analysis

Recent advances in computing technology have allowed previously defined FD calculation algorithms to now be performed much more quickly, and the availability of commercially available software such as ImageJ and SPSS allow for quicker data collection and more precise analysis. This novel combination of test model and fractal

assessment should result in more cohesive data and a better method of diagnosing subject prognosis.

1.3 Infiltrate analysis background

In addition to fractal analysis, a count of the inflammatory infiltrate cells that populate regions just inside of the epithelial layer can be an indicator of tumor development (Thomas, Matthews et al. 1995, Balkwill and Mantovani 2001). The shift in inflammatory infiltrate from low (associated with dysplasia) to high (more typical of OSCC) is related to a loss in function of various immune cell populations during oral carcinogenesis, induced by a PAH. Inflammatory cells that appear in the tumor environment and contribute to cancer growth include dendritic cells, lymphocytes and macrophages, which produce growth factors that harm the extracellular matrix, increasing tumor production, invasion, and metastasis. Additionally, inflammatory cytokines can significantly increase DNA damage and the negative regulation of tumor-suppressing protein p53 (Balkwill and Mantovani 2001).

1.4 Clustering background

In order to perform classification of tissue samples, relevant features must be extracted from photographs of each sample. These features are obtained through the aforementioned processes, fractal analysis and inflammatory infiltrate analysis. By using the guide to pattern of tumor invasion (POI), the images can first be classified

based on standard pathologic methods. These images are called training samples, and correlating the POI classifications with the fractal analysis and inflammatory analysis classifications will allow the data to be plotted in a feature space where different classifications are separated by decision boundaries. On a plot, these classifications are often known as clusters (Duda, Hart et al. 2001).

Duda and Hart's classic analogy explains this nicely. If a fish-packing plant that wants to automate the process of sorting fish according to species, such as sea bass and salmon, it might use pattern classification. The plant might set up a camera to allow an observer to note physical differences between the two types of fish, using features such as length, width, lightness, and fin shape. Each species would have a separate model, or form that could be described mathematically. As the camera extracts more features, a classifier can be generated to make a decision on whether a particular incoming fish belongs to the category of sea bass or salmon. The data used to create this classifier is known as training data, and should generally become more accurate as more data points (fish, in this case) are analyzed. The goal of the training data is to have enough data to create a classifier that will correctly classify the fish often enough to surpass some predetermined threshold (Duda, Hart et al. 2001).

2. HYPOTHESIS

The purpose of this study is to examine the effectiveness of combining various methods of fractal dimension analysis and inflammatory infiltrate analysis in order to accurately discriminate between normal epithelium, multiple stages of epithelial dysplasia, and OSCC when applied to a controlled carcinogenesis model in Syrian hamsters. We believe this process can significantly reduce inter-observer variability, allowing for more accurate diagnosis and the application of appropriate treatment methods to improve long-term prognosis.

Specifically, it will measure the applicability of different methods of fractal analysis (box counting, full tissue scans, and tissue subscans) and of infiltrate analysis (infiltrate count, total infiltrate area, average cell size, and area fraction). It will correlate the results of this mathematical analysis with those obtained by an experienced pathologist through the application of a conventional histopathological classification system for such lesions, based on established criteria for assessment of the pattern of tumor invasion.

3. METHODS

3.1 Hamster oral carcinogenesis studies

As a precursor to this experiment, a study was conducted at the Institute for Cancer Prevention (part of the National Cancer Institute) by Dr. Joel Schwartz, which observed the effects of carcinogen application on Syrian hamsters (*Mesocricetus auratus*). The study separated the animals into three treatment groups: acetone vehicle control, benzo[a]pyrene (B[a]P), and dibenz[a,l]pyrene (DBP). Each animal was treated three times a week for 40 weeks through application of the carcinogen to the lateral border of the tongue (right side) and floor of the mouth. Histopathologic assessment as well as an assessment of DNA damage and repair were conducted, and ultimately this study demonstrated that an uninhibited application of 0.02 nM application of DBP to hamsters would lead to tumor development in nearly all animals (Schwartz, Baker et al. 2004).

This observation led to a study conducted at UIC by Dr. Schwartz in 2005, from which the tissue samples for this project were taken. This study included a control group, a 1.0 nM B[a]P group, and three groups with DBP applied in varying concentrations of 0.025 nM, 0.0025 nM, and 0.00025 nM. These groups included 25 animals each and were investigated for cancer induction of oral squamous cell carcinomas after 15 weeks and 25 weeks of application. Animals were euthanized after the development of tumors, and samples of epithelial tissue were taken from the floor of the mouth, the lateral border of the tongue, and the buccal pouch of each animal.

Groups	Number of Mild Cases	Number of Moderate-Severe Cases
Acetone Control	0/15	0/15
BP	6/15	4/15
DBP	8/15	8/15

Table 1. Histopathology for dysplasia following exposure to BP, DBP (tongue)

Groups (25 animals/group)	Week 25 Mean Tumor Volume (mm³)	Week 35 Mean Tumor Volume (mm³)
Acetone	0.0	0.0
B[a]P (1.0 nmol/app)	95.6	127.5
DBP (0.025 nmol/app)	1018.8	17e3
DBP (0.0025 nmol/app)	510.2	642.8
DBP (0.00025 nmol/app)	104.8	140.3

Table 2. Incidence of tumor formation by treatment

The tissue samples were fixed using 10% neutral buffered formalin before being dehydrated and cleared. The samples were then embedded in paraffin and sectioned into slices 5-6 microns wide, prior to being stained with a combination of hematoxylin and eosin (H and E staining) and placed in coverslips.

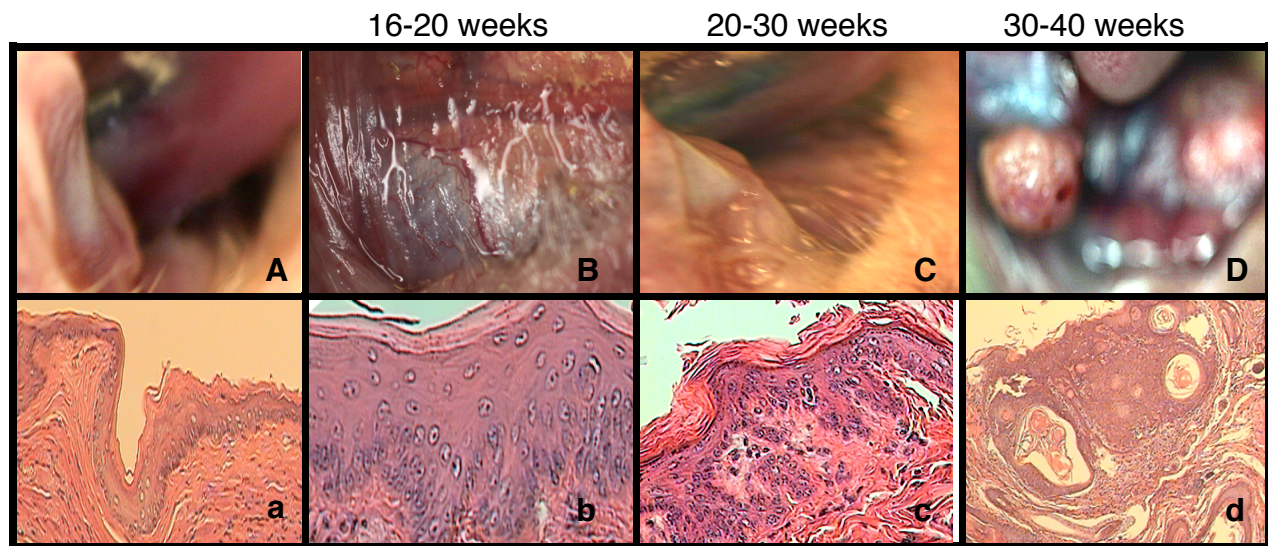


Figure 1. Change in oral mucosa with application of dibenz[a,l]pyrene

A = normal oral mucosa
a = normal histology
B = leukoplakia
b = hyperplasia
C = early oral mass
c = early invasive cancer
D = tumor mass
d = deeply invasive

3.2 Slide analysis

3.2.1 Slide conversion to digital format

In order to analyze the fractal dimension of the epithelial layer of each tissue sample, the slides needed to be converted to a digital format. This was accomplished using a Leica light photomicroscope equipped with a SPOT camera system. This microscope is equipped with objectives with magnifications of 10X, 20X, and 40X.

3.2.2 Fractal analysis procedure

After converting to a digital format, the images were modified so that the epithelial layer would be the focus of the image. In order to do this, the RGB images needed to be converted using ImageJ, first to a grayscale format, and then to a binary image to reveal the edges of the epithelial layer (Rasband 2009). This process is shown visually in Figure 2.

Converting from grayscale to binary required the user to properly threshold each image in such a way that the boundary epithelial layer would not be lost, while at the same time removing as much unnecessary information from the image as possible. With the thresholding process completed, ImageJ could find the edges in the binary image, allowing the user to select the epithelial layer boundary as the region of interest (ROI) for the fractal calculation.

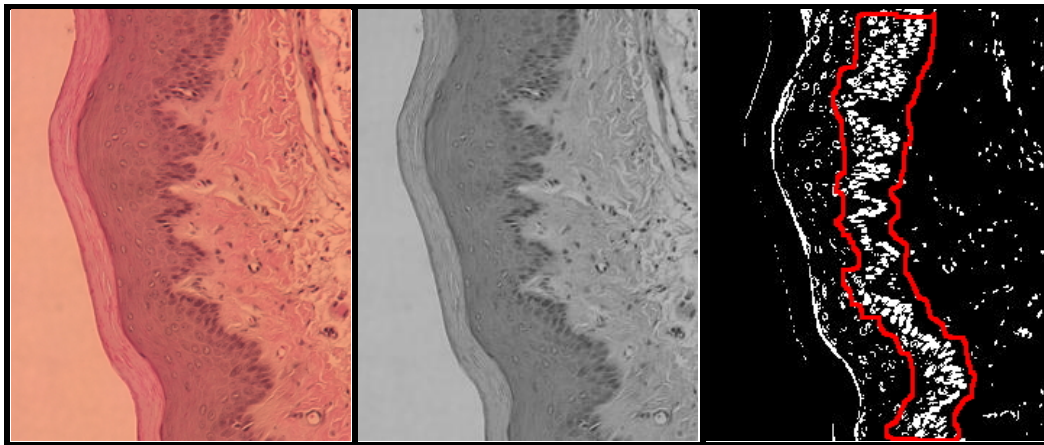


Figure 2. Conversion process of digital slides through steps: 1, original image; 2, grayscale; 3, thresholded to emphasize epithelial layer, ROI circled in red

The basic algorithm for finding the FD of an image uses the following formula:

$$N \propto \varepsilon^{-D_F}$$

Equation 2

In an irregularly-shaped line whose FD is being calculated, N represents the number of pieces which the line can be broken into when using pieces of scale ε . This leaves D_F as the fractal dimension. Solving for D_F leaves the equation:

$$D_F = \log N / \log \varepsilon$$

Equation 3

The FracLac plugin was used to perform the fractal dimension calculations for this project. FracLac, a free add-on for ImageJ, allows for the calculation of fractal values using a number of existing algorithms and the ability to change multiple calculation settings (Karperien 2007).

3.2.2.1 Simple box count

One common algorithm used to obtain fractal dimension is the simple box count, which takes the slope of the above equation, determining how number of parts N changes with scale ε (calculated in this case as [box size/image size]) thus giving:

$$D_B = \text{the slope of } (\ln N / \ln \varepsilon)$$

Equation 4

where D_B is the box-counting dimension. FracLac allows for the calculation of D_B based on parameter settings that determine how many different values of N and ε will be used (Karperien 2007). From a more visual standpoint, the algorithm lays a series of grids of decreasing box size over the image, and counts the number of boxes that contain portions of the image for each box size.

Box count, in addition to FD, also gives each image a value of lacunarity, which is a measure of texture in a feature. An image that is closer to being homogenous and to having a translationally and rotationally invariant pattern will have a lower value of lacunarity, given as λ . Patterns with similar fractal dimensions can often be distinguished by their lacunarity, which is determined by the following, more complex formula:

$$\lambda_{\varepsilon,g} = CV_{\varepsilon,g}^2 = (\sigma_{\varepsilon,g} / \mu_{\varepsilon,g})^2$$

Equation 5

where λ represents the lacunarity for each grid of caliber ε (as above) calculated from the standard deviation σ and mean μ of pixels per box for each grid orientation g (grid orientation is the variable location of the box grid laid over the ROI).

A total of 55 images at 1600 x 1200 pixels were captured at 20X and analyzed using the simple box count. The FracLac settings for box counting used boxes that ranged from a minimum of two pixels in size to a maximum size of 45% of the ROI.

3.2.2.2 Subscans

Another algorithm FracLac uses in order to determine FD is the process of conducting subscans, calculating local box count dimensions within a single image. Through this method, a scan returns not just a single value for FD and lacunarity, but tens or hundreds of values, depending on user options which determine how many separate scans are done within the specified ROI of each image.

The most efficient way to perform a subscan is to use the same process of converting the image into a binary, and then to use edge detection, as was done for a box count. Within the scan type option for subscans in FracLac, the best choice in terms of both computation time and accuracy is a rectangular scan, which uses an array of squares, computing FD and lacunarity of each.

Three other key settings were varied for the subscans as well, these being the number of box sizes used per scan, the sample size (given as the length of a side of a square in pixels), and the size of the largest box as a percentage of the total ROI size.

Using a high number of boxes per scan gave a much higher computation time per image, whereas using too small a number would result in wildly inconsistent values for FD and lacunarity. For the purposes of this test, five box sizes per scan gave the most reasonable values in a relatively short period of time (on the order of a few minutes per image, rather than ~1 hour).

Similarly, a subscan consisting of squares that were 300 x 300 pixels would not accurately provide enough data for a ROI of just a few hundred pixels in width and length. A subscan of 50 x 50 squares was better in terms of coverage, but the tradeoff

in terms of accuracy did not improve enough to offset the extra computation time over using 100 x 100 squares.

Setting the maximum box size was also an important consideration when performing subsamples. It is important not to set the maximum box size above 50% of the total ROI, because of the greater chance of errors (Rasband 2009). Using an upper limit of the default setting of 45% of ROI down to a lower limit of 10% of ROI, various tests were performed. The lower settings resulted in noisier data, most likely because the required slope of $(\ln N / \ln \epsilon)$ did not cover a wide enough range of grid calibers. A midpoint value of 25% was chosen, as it yielded the most meaningful results and would ensure that there was an adequate range of grid sizes chosen.

Subsamples were performed on 42 of the sample images, with resulting values stored in a spreadsheet for each image. In order to perform a correlation, the sets of values for the FD and lacunarity had to be averaged, using an arithmetic mean as well as a weighted mean. For the weighted mean, because early correlations had shown that higher FD values corresponded to a higher POI value, it was decided to weight the higher FD values and perform an average that way. The top ten FD values were taken, averaged, and used as the weighted value of the FD for the subsample. A similar process was performed to obtain a weighted value of the lacunarity.

3.2.2.3 Full tissue scans

A third method of performing scans involved lowering the magnification from 20X to 10X in order to capture an entire segment of tissue, rather than just a portion of the

epithelial layer. Due to limitations in the image capture size, most tissues required anywhere from two to eight separate images in order to capture the entire sample.

Each section of the tissue had its fractal dimension and lacunarity calculated from the box counting algorithm, using the same procedure for converting the image to binary and emphasizing the epithelial layer as outlined in the box count method above. A new set of 20 tissue samples was analyzed this way, resulting in 70 images. These tissues were taken from a variety of sites including the lip, salivary glands, floor of the mouth, and tongue.

3.2.3 Inflammatory infiltrate analysis

In addition to fractal analysis, correlation with the density of inflammatory infiltrate cells that populate regions just inside of the epithelial layer was also useful to examine. Though not strictly a fractal-based analysis, inflammatory infiltrate cell count is useful in pathologic diagnosis of neoplasia, and could potentially prove useful in this analysis. The inflammatory infiltrate consisted of lymphocytes, histiocytes (tissue type), and granulocytes (eosinophils, basophiles, mast cells, and polymorphonuclear cells).

In order to perform this procedure, the RGB image of the slide was converted to grayscale as before, but this time the image was thresholded to emphasize the inflammatory cells. These cells represented the portion of the image that would be the ROI for the cell count. From this point, the Analyze Particles feature in ImageJ was used to count the cells and their sizes. This procedure was performed on a subset of the original group of images, yielding information including infiltrate cell count, infiltrate

area (in pixels²), average infiltrate cell size (pixels²), and area fraction (%) of the image covered by infiltrate cells.

3.2.4 Classifying by pattern of tumor invasion

Histopathologic classification by an experienced pathologist depends on a number of factors when any tissue sample is examined. As an aid, a guide to classifying histopathology based on pattern of tumor invasion (POI) was used (Brandwein-Gensler, Teixeira et al. 2005). Although the guide was originally intended for use with human tissue, its categories translate well to analyzing oral hamster tissues given the controlled nature of the experiment, using genetically-similar hamsters that were injected with controlled doses of DBP and are genetically similar. As pictured in Figure 3, our modified POI guide identified five categories of neoplasia in the hamster group.

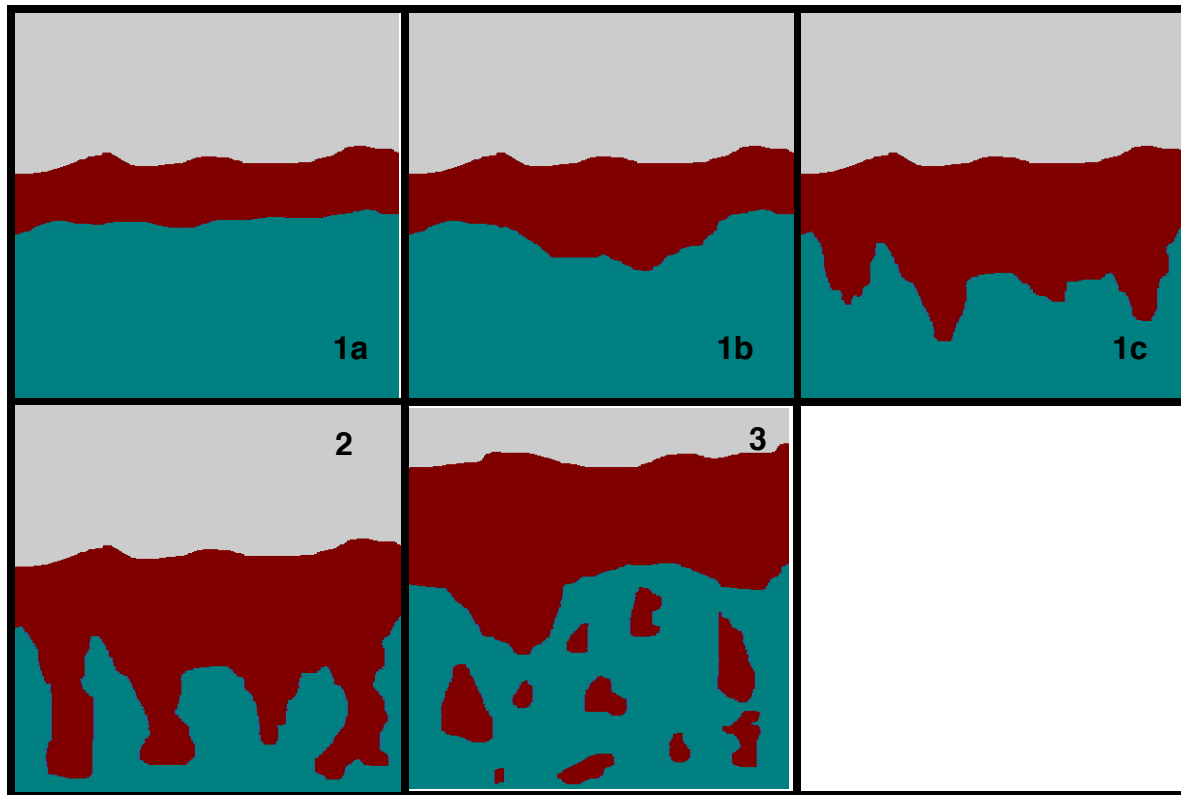


Figure 3. Patterns of tumor invasion based on epithelial structure, 1a (normal tissue), 1b (mild dysplasia/hyperplasia), 1c (moderate/severe dysplasia), 2 (carcinoma *in situ*, early OSCC), 3 (invasive OSCC). (Based on a presentation from Brandwein-Gensler, 2011.)

POI 1 represents a broad, invasive front of cell growth. This may be mostly normal cell growth, or may represent mild forms of atypia and/or hyperplasia. Within this category, three separate subcategories were created to distinguish normal tissue from tissue that shows some signs of irregular growth, leading to names 1a, 1b, and 1c. 1a represents a normal epithelial layer showing virtually no signs of irregular growth. 1b shows hyperplasia or mild dysplasia isolated to a single region of several cells, whereas 1c shows moderate to severe dysplasia in multiple regions, often along a significant portion of the epithelial layer.

POI 2 represents a finger-like pushing front, with a stellate appearance. It tends to show early signs of OSCC.

POI 3 represents tumors that develop into islands (greater than 15 cells each) after breaking away from the original epithelial region. This is considered to represent invasive OSCC and is among the most severe categorizations for the hamster tissue.

In addition, there exist POI 4 and POI 5 (not pictured), which are considerably more severe. Due to the euthanization of hamsters upon development of cancer in order to reduce pain, as per the animal care committee requirements, these categories are not observed in these particular samples.

In order to classify the tissue samples to a specific POI, the Brandwein-Gensler guide was used to examine the epithelial layer and categorize the tissues accordingly. These categories were used accordingly in order to determine correlation when compared to the FD values.

3.2.5 Statistical data analysis

IBM SPSS Statistics was used to process data for the two image sets. Each image had its POI listed based on the guide to pattern of tumor invasion (Brandwein-Gensler, Teixeira et al. 2005). This POI ranging from 1a to 3 was converted to a numerical value between 1 and 5 for more logical processing. The box count FD and box count lacunarity were listed, as well as two sets of subscan FD and lacunarity: the average FD and lacunarity taken as the arithmetic mean of all values calculated in the

subscan, as well as a weighted value which took the top ten values of FD and lacunarity and calculated the arithmetic mean of those values. In addition, inflammatory infiltrate values were added, specifically the total cell (whole particle) count for the ROI, the total area covered as part of the ROI, average cell size within the ROI, and the area fraction, determined as the percentage of pixels counted as infiltrate within the ROI (Rasband 2009).

In order to determine which variables were most closely correlated with each other, it was determined that a Spearman correlation would be performed. The Spearman rank correlation coefficient, given as ρ (and often referred to as Spearman's rho), is a non-parametric measure of statistical dependence for two variables, with a range from -1 to +1. A value of +1 indicates a perfect, monotonic positive correlation, whereas a value of -1 indicates a perfect, monotonic, negative correlation. A value of 0 indicates no correlation at all. Determining the most correlated variables will allow a hierarchical cluster process to be performed, making it possible to accurately determine POI of a tissue image based on multiple variables (Sarstedt and Mooi 2010).

3.2.6 Advanced statistical data analysis

Advanced statistical analysis methods can help better demonstrate the strength of evidence provided by FD and lacunarity that allow classification into the various POI categories.

3.2.6.1 Two-step cluster analysis and ANOVA

More advanced forms of cluster analysis can take the existing variables that are calculated for each data point (FD and lacunarity, to begin with) and attempt to combine them into groups based solely on a mathematical algorithm, independently of any outside observations. The analysis can then evaluate how those newly created groups form any natural patterns with respect to observed POI.

In order to mathematically separate the data points into discrete clusters, an algorithm known as two-step clustering (TSC) can be used. TSC is considered the best method of cluster analysis for data that includes a combination of categorical and continuous variables (IBM SPSS Statistics 2013).

The TSC process starts by scanning the data points and determining, based on a distance calculation, whether each point should be part of a new cluster or should merge with an existing cluster. These pre-clusters are then recursively merged by determining their distance from one another and combining those that are closest together. This proceeds until either the pre-determined number of total clusters is reached, or until the software determines the optimal number of clusters based on maximization of distances between all clusters (IBM SPSS Statistics 2013). In this case, the number of clusters is preset to five in order to mirror the POI categories.

The one-way analysis of variance, or ANOVA, is used in this situation to determine the statistical significance by calculating the p-value of the POI between the clusters. In other words, it will determine whether there is a difference between the values and means of the data points in each of the clusters that cannot simply be explained by sampling error (Urdan 2010).

3.2.6.2 Receiver operating characteristic

The receiver operating characteristic (ROC) curve is used to determine the rate of false positives (Type I error) and false negatives (Type II error). ROC calculates both the sensitivity and specificity of a method of pattern classification. The principle was initially used during World War II as a method of determining whether objects detected via radar were enemy targets, friendly, or simply noise in the signal detection process. ROC analysis since the 1970s has widely been used in medicine and radiology, as well as in fields including data mining research (Liu and Bandos 2012).

The output known as the area under the curve (AUC) is a measure of diagnostic accuracy, ranging in value from 0.5, which represents the same accuracy as a random guess, to 1.0, which is perfect accuracy (Liu and Bandos 2012). The ROC curve is typically used to illustrate the performance of a purely binary classifier system, such as a medical diagnosis outcome of either positive or negative. Because of this limitation, the best method for determining AUC in this case was to perform a separate ROC calculation on each of the five POI categories. All data points had to be re-categorized separately for each POI, given a value of “1” if that was the observed POI, or “0” if it was not. In addition, the ROC procedure had to be run twice for each of the five POI categories—once with FD as the test variable, and once with lacunarity as the test variable.

4. RESULTS

4.1. Hamster carcinogenesis results

The hamster study at UIC was conducted to determine presence of histopathologic change before the 25-week treatment time point. After 10, 15, or 25 weeks animals were euthanized for gross and histopathologic examination to determine whether dysplasia or OSCC had developed. Hamsters that received 10 weeks of treatment, regardless of the application using B[a]P or DBP, showed no gross tumor masses.

Following DBP application, twenty animals developed premalignant or malignant changes, which were situated in the floor of the mouth and less frequently in the buccal pouch. Fifteen weeks after the start of treatment, 5/7 randomly selected animals had squamous carcinoma. Ten weeks afterwards, a repeat of this process produced 7/7 animals with squamous carcinoma in the floor of the mouth extending towards the lip.

4.2 Fractal dimension and lacunarity results

Running a Spearman correlation allowed us to determine how closely values such as fractal dimension and lacunarity were related to the diagnosed POI. The Spearman rank of the box count FD versus the POI was 0.791 ($p < .001$), and the rank of the lacunarity versus the POI was -0.694 ($p < .001$). (The general rule is that for the result to be statistically significant, the p-value, or probability that the null hypothesis of there being no correlation between the data is correct, should be less than .05 (Stigler

2008, Caldwell 2009)). This meant that the FD had a strong, positive correlation to the POI, whereas the lacunarity had a strong, negative correlation to the POI. The boxplot in Figure 4 demonstrates the range in box count FD for POI categories 1a through 3. Figure 5 shows the same range for box count lacunarity.

POI	Count	Mean FD	Std Dev FD	Min FD	Max FD	Mean Lac	Std Dev Lac	Min Lac	Max Lac
1a	3	1.582	0.08	1.493	1.646	0.555	0.082	0.479	0.641
1b	13	1.664	0.063	1.547	1.774	0.587	0.154	0.336	0.798
1c	14	1.695	0.094	1.426	1.785	0.535	0.179	0.298	0.961
2	12	1.793	0.057	1.723	1.922	0.389	0.091	0.224	0.558
3	13	1.81	0.026	1.77	1.853	0.322	0.087	0.199	0.448

Table 3. Box count fractal dimension and lacunarity classified by pattern of tumor invasion

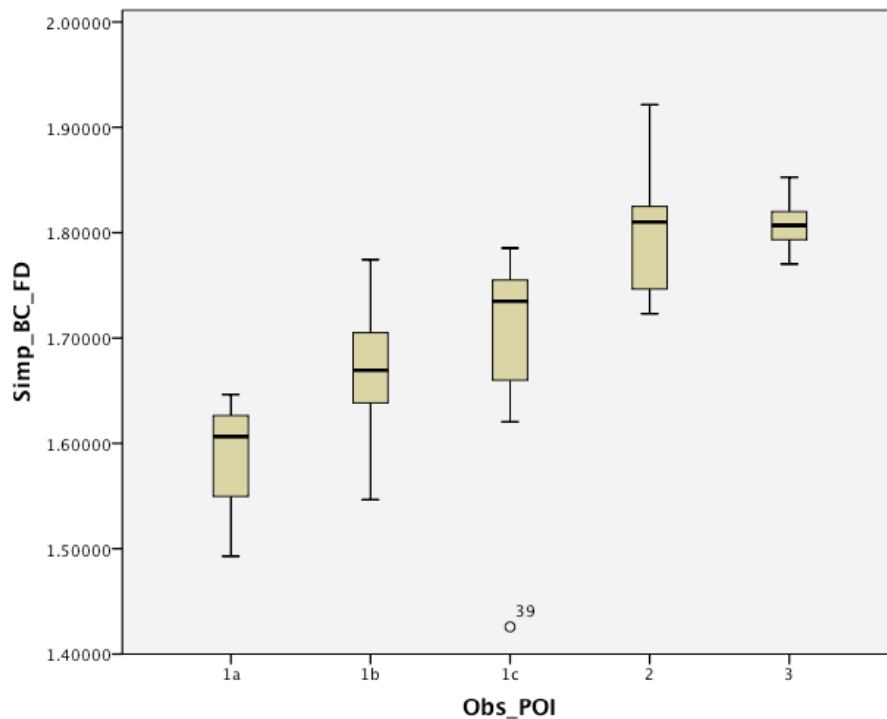


Figure 4. Simple box count FD grouped by POI

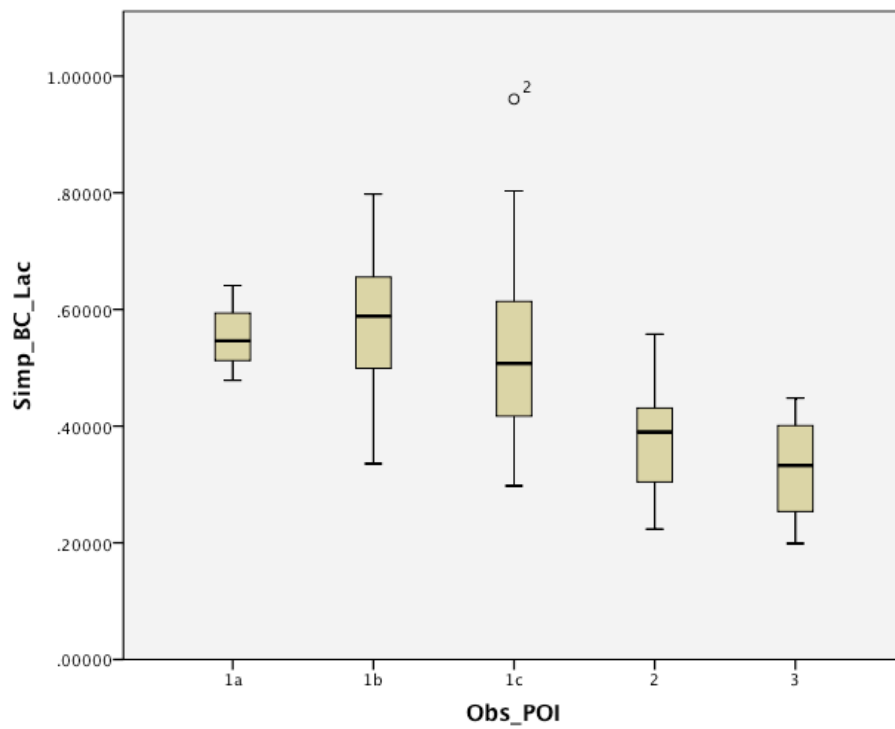


Figure 5. Simple box count lacunarity grouped by POI

The 1a POI category consisted of three samples with a mean box count FD of 1.582. The highest value was 1.646 while the lowest value was 1.493. The box count lacunarity had a mean of 0.555 and a total range from 0.479 to 0.641.

Category 1b had 13 samples with a mean FD of 1.664 with a range from 1.547 to 1.774. The lacunarity had a mean of 0.587, ranging from 0.336 to 0.798.

Category 1c was composed of 14 samples and had a mean FD of 1.695, with a minimum value of 1.426 and a maximum of 1.785. The lacunarity had a mean value of 0.535 with a minimum of 0.298 and a maximum of 0.961.

Category 2 consisted of 12 samples and had a mean FD of 1.793 over a range between 1.723 and 1.921. The mean lacunarity was 0.389 and had a minimum of 0.224 and a maximum of 0.558.

Category 3 included 13 samples with a mean FD of 1.810 and a range of 1.770 to 1.853. The lacunarity had a mean of 0.322 with a range of 0.198 to 0.448.

Combining the data to show both box count FD and lacunarity on the same plot with POI represented by different colors allows the data to be clustered in two dimensions, and gives a better idea of the relationship between the two values. This plot is shown in Figure 6.

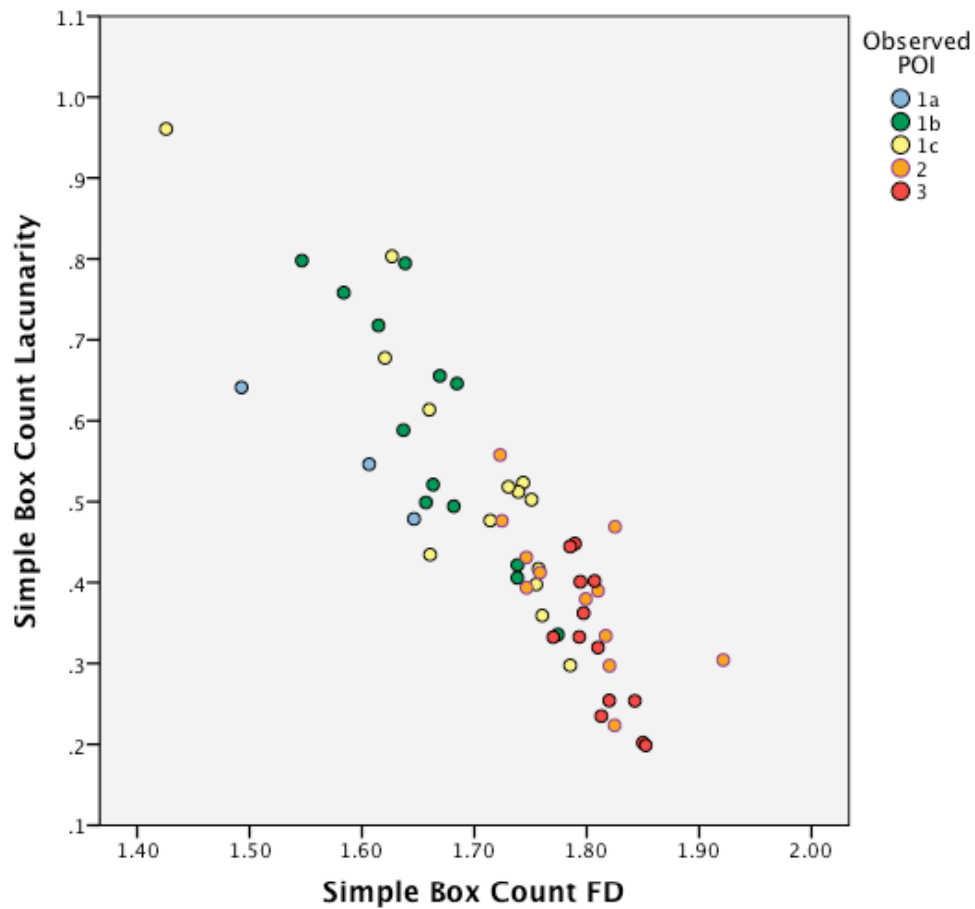


Figure 6. Box count fractal dimension and lacunarity scatter plot grouped by POI

A Spearman correlation was also performed to determine whether the subscan method would be useful in determining POI. Due to the time required to perform a single subscan, a random selection of 42 images was used to perform the initial Spearman correlation, with a view to using the entire set of images if this subset yielded a substantial improvement over the simple box count method. Using the mean method, Spearman rank for the FD versus the POI was 0.653, and rank for the lacunarity versus

the POI was -0.660. Using the weighted subscan method resulted in FD versus POI Spearman rank of 0.678, and -0.393 for lacunarity versus POI.

Since the subscan methods actually yielded weaker Spearman ranks than the simple box count method, and considering the extra time it took to perform a subscan (20-60 minutes, depending on scan settings, versus < 5 minutes for a standard box count), this method of FD analysis did not produce significant results.

The full scans were performed on a sample of 90 images that were taken from 20 tissue slides. For each slide, FD and lacunarity were calculated for each section and then averaged to get a total FD and lacunarity value for each slide. The Spearman ranks for FD and lacunarity versus POI were 0.253 and -0.004, respectively. Again, due to poor correlation results, it did not make sense to proceed with this method.

4.3 Inflammatory infiltrate results

For the inflammatory infiltrate analysis, not every image had easily identifiable infiltrate, thus there are fewer samples that were included. A total of 33 images were categorized using inflammatory infiltrate analysis.

POI category 1a consisted of three samples with a mean infiltrate count of 90, a mean total infiltrate area of 4269.33, mean average cell size of 62.35 and a mean area fraction of 8.58.

Category 1b included six samples with a mean infiltrate count of 153.67, a mean total infiltrate area of 5298.33, mean average cell size of 38.05 and a mean area fraction of 3.40.

Category 1c included six samples with a mean infiltrate count of 27.50, a mean total infiltrate area of 1157.17, mean average cell size of 44.61 and a mean area fraction of 4.64.

POI	Count	Mean Inf Count	Std Dev Inf Count	Mean Inf Area	Std Dev Inf Area	Mean Avg Cell Size	Std Dev Avg Cell Size	Mean Area Frac	Std Dev Area Frac
1a	3	90.00	100.9	4269.3	812.7	62.35	35.43	8.58	5.34
1b	6	153.67	136.8	5298.3	3712.4	38.05	19.75	3.40	2.04
1c	6	27.50	15.80	1157.2	772.5	44.61	18.19	4.64	3.63
2	9	658.56	1015.5	48631.2	72935.6	71.19	21.90	15.67	6.35
3	9	1014.56	586.9	65832.2	38459.9	66.86	8.98	17.51	5.36

Table 4. Inflammatory infiltrate statistics classified by pattern of tumor invasion

Category 2 included nine samples with a mean infiltrate count of 658.56, a mean total infiltrate area of 48631.22, mean average cell size of 71.19 and a mean area fraction of 15.67.

Category 3 included nine samples with a mean infiltrate count of 1014.56, a mean total infiltrate area of 65832.00, mean average cell size of 66.86 and a mean area fraction of 17.51.

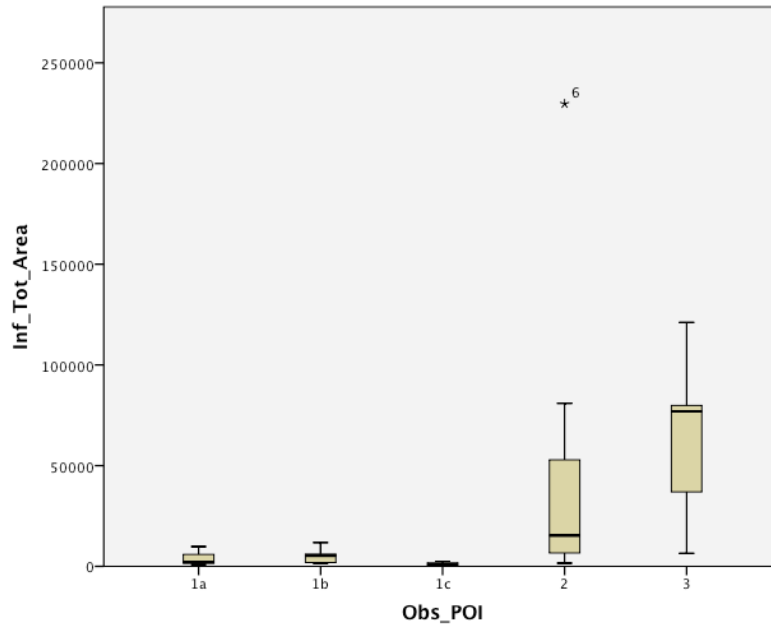


Figure 7. Inflammatory infiltrate total area grouped by POI

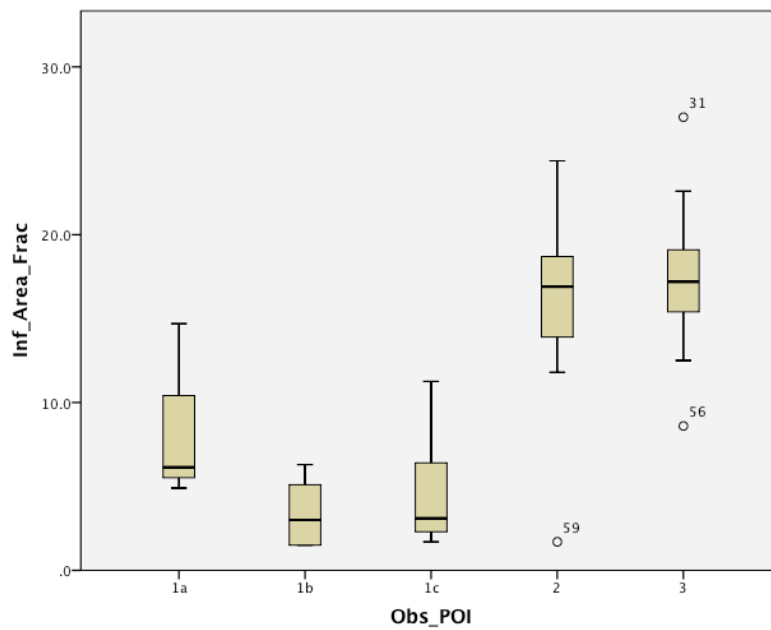


Figure 8. Inflammatory infiltrate area fraction grouped by POI

A Spearman correlation can also be performed with inflammatory infiltrate information, with varying results. Spearman rank for the total infiltrate count, a measure of the total number of infiltrate cells in a given image, versus POI was 0.606. Similar Spearman ranks calculated for total infiltrate area (area covered by infiltrate cells), average size of infiltrate cells, and infiltrate area fraction (total percentage of image covered by infiltrate cells) were, respectively, 0.676, 0.402, and 0.674. Therefore total infiltrate area and infiltrate area fraction provided the best overall correlation to POI.

As was shown before, taking multiple values into consideration at once allows for clustering to be performed. Using the statistics that yield the strongest Spearman correlation gives cluster data as seen in Figure 9.

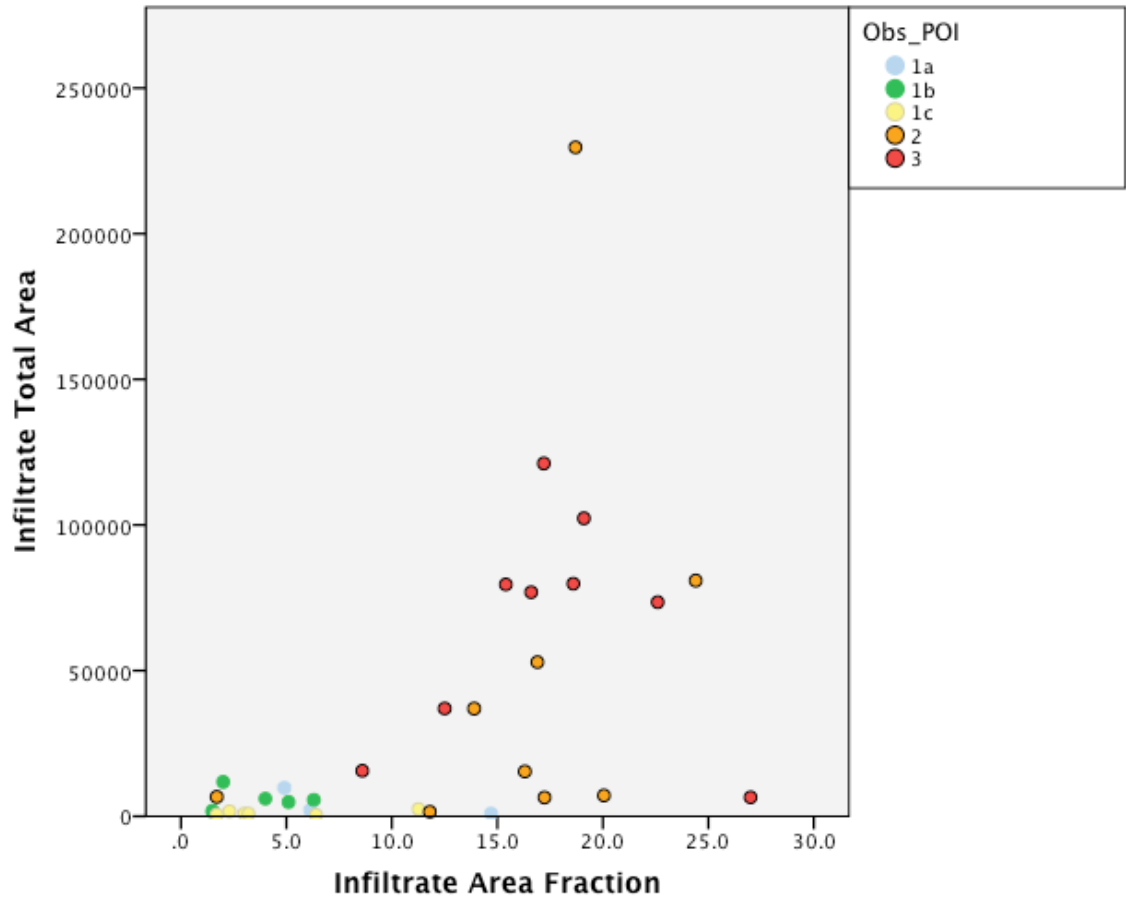


Figure 9. Inflammatory infiltrate total area and area fraction scatter plot grouped by POI

4.4 Advanced analysis results

Performing a two-step cluster analysis while setting the required number of clusters to five yielded a group of clusters with distinct differences, as well as some similarities. Comparing the mean values of the input variables for each cluster's data points allows this to be seen.

For the purposes of this cluster analysis, POI categories 1a, 1b, 1c, 2, and 3 have been translated to numbers 1 through 5, in ascending order. This allows for easier calculations of the average POI for each cluster.

The first cluster created by the two-step procedure has a FD of 1.57, a lacunarity of 0.77, and it corresponds to data points that have an average observed POI of 2.25. Of a very similar nature is the second cluster, with a FD of 1.66, a lacunarity of 0.55, and data points with an observed POI of 2.00. Both of these clusters share the characteristic of a lower FD, medium to high lacunarity, and correlate with having low values of observed POI.

The third cluster has medium values of FD and lacunarity, at 1.74 and 0.46, respectively. The observed POI of its points is also at a medium level of 3.21.

The fourth cluster has a FD of 1.79 and lacunarity of 0.37. Its data points correspond to an observed POI of 4.27. Very similarly, the fifth cluster has a FD of 1.84, lacunarity of 0.25, and a high observed POI of 4.62. Both of these clusters have a higher FD, lower lacunarity, and correlate to a higher average observed POI.

The result of a one-way ANOVA using observed POI as the dependent variable and cluster classification as the factor yields a significance of $p < .001$. Thus, the cluster-based results can be considered quite statistically significant.

Receiver operating characteristic curve results are as shown in the tables below, with results showing a statistically significant level of $p < .05$, except as noted. Although several of these were only slightly higher than .05, that is the value that is typically considered as the appropriate cutoff (Stigler 2008).

POI	Area Under the Curve	95% Confidence Interval
1a	0.923	0.835 – 1.000
1b	0.815	0.702 – 0.928
1c	0.670*	0.529 – 0.811
2	0.753	0.611 – 0.895
3	0.875	0.785 – 0.966

Table 5. Fractal Dimension ROC Curve Results

POI	Area Under the Curve	95% Confidence Interval
1a	0.744*	0.602 – 0.885
1b	0.784	0.648 – 0.920
1c	0.666*	0.509 – 0.822
2	0.680*	0.534 – 0.827
3	0.857	0.755 – 0.960

Table 6. Lacunarity ROC Curve Results

*p > .05; not considered statistically significant

For reference, AUC above 0.9 is considered excellent accuracy of a diagnostic test, with 0.8 to 0.89 considered good, and 0.7 to 0.79 considered fair. The confidence interval represents where the AUC for the total population lies, with 95% confidence.

5. DISCUSSION

5.1 Hamster model and fractal-based analysis

The novel nature of this study is due to the use of a controlled oral carcinogenesis standard tumor model with a combination of several unique factors. These include as previously stated FD, lacunarity, POI, inflammatory infiltrate, and cluster analysis. Although a number of previous studies have investigated FD among tissue sections from OSCC for the purpose of improved diagnosis, these studies did not use our general approach to evaluate under controlled conditions the value of FD under controlled conditions analysis to enhance histopathology.

A controlled environment was created to give syngeneic hamsters regular doses of both B[a]P and DBP. Existing studies involving FD for cancer analysis use human tissue, which as stated in the background section, poses its own set of issues in that carcinogenesis and subsequent tumorigenesis is more complex. Humans are exposed to many different carcinogens, rather than a controlled amount, and tumor biopsy material selection will vary because of clinical and surgical needs. Furthermore, processing of tissue sections will alter FD because of numbers of sections prepared and a variety of origins from tumor surfaces.

Changes were reflected in the histopathology of both groups. The decision was to evaluate FD and associated histopathologic criteria in DBP treatment group tissues because we had recorded the highest level of tumor burden, and OBC analysis disclosed marked changes in cells compared to the B[a]P carcinogen treatments.

To validate these OBC results we used specific criteria developed by Brandwein-Gensler et al to classify histopathologic diagnoses. The criteria created a simple method for classifying histopathologic changes using photographs of the hamster tissue samples. No existing studies have looked at using fractal analysis from a standpoint of dysplastic change as related to Brandwein-Gensler's POI guide, or categorized existing cancer into stages from I to IV (Kikuchi, Kozuma et al. 2002, Goutzanis, Papadogeorgakis et al. 2008). Tissue sections have been examined for fractal analysis to differentiate between benign and malignant masses in previous studies (Esgiar and Chakravorty, Chang, Chen et al. 2004). Some cancer studies have used radiographic images from methods such as ultrasound, which do not provide sufficient detail to detect dysplastic changes. Other studies rely exclusively on fractal dimension, and do not factor in lacunarity or analyze characteristics such as inflammatory infiltrate (Kikuchi, Kozuma et al. 2002, Chang, Chen et al. 2004, Goutzanis, Papadogeorgakis et al. 2008). Furthermore, there is no discrimination of cellular biologic and molecular activities that would validate FD analysis as we showed using OBC sampling.

Procedures were tested to vary the simple box count FD, but this long-standing approach proved to be most useful in distinguishing normal tissue (POI 1a) from more dysplastic and hyperplastic tissues (POI 1b and 1c), as well as distinguishing those tissues from early stages of cancer and OSCC which are seen in POI 2 and 3. There is a significant overlap in these criteria for categories 1b and 1c, and significant, though

less, overlap between those categories and 1a. Categories 2 and 3 show little FD overlap overall with POI 1a, 1b, and 1c, and thus can be diagnosed more easily.

Box count lacunarity was not an effective means to distinguish between POI 1a, 1b, and 1c, or to discriminate between POI 2 and 3. However, lacunarity was able to distinguish POI 1 categories with normal or slightly hyperplastic or dysplastic tissue from POI categories 2 and 3, which show more signs of early cancer.

Taking the values of box count FD and lacunarity together allows us to form clusters to more accurately diagnose tissue samples. The cluster of POI 1a is categorized by a combination of medium lacunarity and low fractal dimension. Clusters for 1b and 1c are similarly shown to have a combination of low to medium FD and a mean lacunarity that is medium, although it has a significant standard deviation. Clusters for POIs 2 and 3 are categorized almost exclusively by FD at the upper bound as well as a much lower lacunarity. As expected, there is significant overlap of the two clusters of data, although POI 3 tends towards higher FD and lower lacunarity.

The clustering process was also performed with inflammatory infiltrate data, to combine information onto a single plot. Observing the values with the best Spearman correlation shows that POI 1a, 1b, and 1c display almost identical characteristics of low infiltrate area and low infiltrate area fraction, while both values increase significantly for POIs 2 and 3, with POI 3 having a higher total infiltrate area.

One of the goals of this study was to dissociate various stages of dysplasia and severe dysplasia from OSCC. This analysis indicates an increase in FD that correlates with the progression from mild to moderate to severe dysplasia. A combination of FD

and lacunarity can aid in dissociating normal tissue, mild to moderate dysplasia, and early OSCC from one another. In addition, the study of inflammatory infiltrate can help differentiate mild or moderate dysplasia from OSCC.

Although histopathologic characteristics such as the degree of inflammatory infiltrate appear at first to add confusion, this assessment in fact contributes to our understanding of quantitative changes occurring in the Syrian hamster during oral carcinogenesis. By using a combination of FD, additional mathematical validation, and established histopathologic criteria, we observed the improvement of histopathologic assessment of neoplasia.

5.2 Uses of advanced statistics

Through the use of two-step clustering (TSC), we defined five distinct clusters based solely on the measured variables of FD and lacunarity. These defined clusters corresponded extremely well to the observed patterns of invasion defined by Brandwein-Gensler's criteria. This provides strong evidence that fractal dimension criteria can be used to emulate and improve upon the analysis of a trained pathologist when it comes to histopathologic diagnoses. The advantage of this method is that it allows the clusters to be used for classification of future dysplastic tissue datasets, since it mathematically calculates the mean FD and lacunarity of each cluster. Any new data points obtained in the future can now be classified based on a distance calculation for both of these variables. Alternatively, new data points could be used to further refine

the existing two-step clusters by being added to the original set and performing a TSC algorithm on the newly-expanded set.

There is some deviation from the expected correlation between FD and lacunarity compared to POI at the lower end of the POI scale. For the first two clusters, corresponding to POI 1a and 1b, the FD for 1b is slightly lower, while the lacunarity is slightly higher. This may be attributed to relatively few values in the lower categories of observed POI.

The use of the receiver operating characteristic (ROC) curve resulted in mixed, though not altogether unexpected results. Running an ROC analysis on each POI separately for all the data points serves the purpose of determining the likelihood that a specific point will be incorrectly classified. Although there appears to be a high degree of certainty that FD alone can be used to classify slides that either tend towards POI 1a and 1b or POI 2 and 3, there is far less certainty that the same can be done for slides that fall into category 1c, whose statistical significance falls outside the required criteria of $p < .05$. In addition, lacunarity alone is shown to have weak specificity and sensitivity for most POI classifications. While those AUC tests that fall just outside the $p < .05$ threshold can be held up as evidence of a possible trend, they cannot be appropriately considered to be significant enough on their own to be used in diagnoses. This leads to the conclusion that while neither FD nor lacunarity alone should be used to classify neoplastic tissue slides, both are able to contribute as components of a successful diagnostic model.

5.3 Future aims

In future research it may be useful to repeat the two-step clustering process using a higher number of data points. Ideally, all POI categories should have a similar number of members, at least ten each, and better ability to resemble the real world population as the total number of samples becomes larger.

Other possibilities for future research to build on this study include performing this procedure on human tissue, using a controlled set of biopsy samples for analysis with considerations to correct previously discussed errors. Ideally, there could be a more targeted analysis of cell clones that show signs of dysplasia.

Changes that could be made in analytic techniques include greater automation of the process with image conversion and selection of ROIs by using advanced imaging filters. In addition, more advanced pattern classification methods could be applied, including linear discriminant analysis and multinomial logistic regression.

6. CONCLUSIONS

A number of slides showing various stages of carcinogenesis in Syrian hamsters were classified by severity based on an established pattern of invasion criteria developed by an experienced pathologist. Based upon those categories, a mathematical analysis of these slides using fractal box count and inflammatory infiltrate demonstrated that there are indeed distinct mathematical differences between normal tissue or tissue displaying mild hyperplasia when compared to tissue displaying more severe dysplasia or stages of OSCC.

The statistical significance of these differences in fractal dimension was verified through the use of advanced methods including two-step cluster analysis and the receiver operating characteristic. Thus, fractal dimension analysis has the potential to resolve differences in histopathology that result from inter-observer variability, showing potential to improve the overall accuracy of diagnosis.

CITED LITERATURE

- Abbey, L. M., G. E. Kaugars, J. C. Gunsolley, J. C. Burns, D. G. Page, J. A. Svirsky, E. Eisenberg, D. J. Krutchkoff and M. Cushing (1995). "Intraexaminer and interexaminer reliability in the diagnosis of oral epithelial dysplasia." Oral Surg Oral Med Oral Pathol Oral Radiol Endod **80**(2): 188-191.
- Balkwill, F. and A. Mantovani (2001). "Inflammation and cancer: back to Virchow?" The Lancet **357**(9255): 539-545.
- Brandwein-Gensler, M. (2011). "Validation of the Risk Model in a Low-Stage Cohort" [PowerPoint slides].
- Brandwein-Gensler, M., M. S. Teixeira, C. M. Lewis, B. Lee, L. Rolnitzky, J. J. Hille, E. Genden, M. L. Urken and B. Y. Wang (2005). "Oral squamous cell carcinoma: histologic risk assessment, but not margin status, is strongly predictive of local disease-free and overall survival." The American journal of surgical pathology **29**(2): 167.
- Caldwell, S. (2009). Statistics unplugged, Cengage Learning.
- Chang, R. F., C. J. Chen, M. F. Ho, D. R. Chen and W. K. Moon (2004). Breast ultrasound image classification using fractal analysis, Proceedings of the Fourth IEEE Symposium on Bioinformatics and Bioengineering. 19-21 May 2004.
- Cross, S. S. and D. W. K. Cotton (1992). "The fractal dimension may be a useful morphometric discriminant in histopathology." The Journal of pathology **166**(4): 409-411.
- DELIDES, A., I. PANAYIOTIDES, A. ALEGAKIS, A. KYROUDI, C. BANIS, A. PAVLAKI, E. HELIDONIS and C. KITTAS (2005). "Fractal dimension as a prognostic factor for laryngeal carcinoma." Anticancer research **25**(3B): 2141.
- Duda, R. O., P. E. Hart and D. G. Stork (2001). Pattern classification. New York, Wiley.
- Esgiar, A. and P. Chakravorty Fractal based classification of Colon cancer tissue images, 9th International Symposium on Signal Processing and its Applications. 12-15 Feb. 2007.
- Gianvittorio, J. P. and Y. Rahmat-Samii (2002). "Fractal antennas: A novel antenna miniaturization technique, and applications." Antennas and Propagation Magazine, IEEE **44**(1): 20-36.
- Goutzanis, L., N. Papadogeorgakis, P. Pavlopoulos, K. Katti, V. Petsinis, I. Plochoras, C. Pantelidaki, N. Kavantzias, E. Patsouris and C. Alexandridis (2008). "Nuclear fractal dimension as a prognostic factor in oral squamous cell carcinoma." Oral oncology **44**(4): 345-353.
- Hsü, K. J. and A. J. Hsü (1990). "Fractal geometry of music." Proceedings of the National Academy of Sciences of the United States of America **87**(3): 938.
- Jemal, A., F. Bray, M. M. Center, J. Ferlay, E. Ward and D. Forman (2011). "Global cancer statistics." CA: a cancer journal for clinicians: 2011 Mar-Apr;61(2):69-90.
- Karperien, A. (2007). "FracLac for ImageJ—FracLac Advanced User's Manual." Accessible at <http://rsb.info.nih.gov/ij/plugins/fraclac/fraclac-manual.pdf>. Accessed July 21.

Kikuchi, A., S. Kozuma, K. Sakamaki, M. Saito, G. Marumo, T. Yasugi and Y. Taketani (2002). "Fractal tumor growth of ovarian cancer: Sonographic evaluation." Gynecologic oncology **87**(3): 295-302.

Kujan, O., A. Khattab, R. J. Oliver, S. A. Roberts, N. Thakker and P. Sloan (2007). "Why oral histopathology suffers inter-observer variability on grading oral epithelial dysplasia: an attempt to understand the sources of variation." Oral Oncol **43**(3): 224-231.

Landini, G. (1991). "A fractal model for periodontal breakdown in periodontal disease." Journal of periodontal research **26**(3): 176-179.

Liu, A. and A. I. Bandos (2012). Statistical evaluation of diagnostic performance: topics in ROC analysis, CRC Press.

Mandelbrot, B. "Les objets fractals: forme, hazard et dimension. 1975." Flamarion. Paris.[Links].

Mandelbrot, B. (1967). "How long is the coast of Britain? Statistical self-similarity and fractional dimension." Science **156**(3775): 636.

Mandelbrot, B. B. (1983). The fractal geometry of nature. New York: WH Freeman and Co.

Mani, S. A., W. Guo, M. J. Liao, E. N. Eaton, A. Ayyanan, A. Y. Zhou, M. Brooks, F. Reinhard, C. C. Zhang and M. Shipitsin (2008). "The epithelial-mesenchymal transition generates cells with properties of stem cells." Cell **133**(4): 704-715.

Neville, B. W., D. D. Damm and C. M. Allen (2009). Oral and maxillofacial pathology. (Vol. 620). Philadelphia: Saunders.

Park, N. J., Zhou, H., Elashoff, D., Henson, B. S., Kastratovic, D. A., Abemayor, E., & Wong, D. T. (2009). "Salivary microRNA: discovery, characterization, and clinical utility for oral cancer detection." Clinical Cancer Research, **15**(17), 5473-5477.

Presant, C. A., W. Russell, R. Alexander and Y. Fu (1986). "Soft-tissue and bone sarcoma histopathology peer review: the frequency of disagreement in diagnosis and the need for second pathology opinions. The Southeastern Cancer Study Group experience." Journal of Clinical Oncology **4**(11): 1658-1661.

Rasband, W. S. (2009). "ImageJ, US National Institutes of Health, Bethesda, Maryland, USA." Available at: rsb.info.nih.gov/ij/. Accessed **20**.

Sanders, H. and J. Crocker (1993). "Technical method a simple technique for the measurement of fractal dimensions in histopathological specimens." The Journal of Pathology **169**(3): 383-385.

Sarstedt, M. and E. Mooi (2010). A Concise Guide to Market Research: The Process, Data, and Methods Using IBM SPSS Statistics, Springer Verlag.

Saxen, E., K. Franssila, O. Bjarnason, T. Normann and N. Ringertz (1978). "Observer variation in histologic classification of thyroid cancer." Acta Pathologica Microbiologica Scandinavica Section A Pathology **86**(1 - 6): 483-486.

Schwartz, J., V. Baker, E. Larios, D. Desai and S. Amin (2004). "Inhibition of experimental tobacco carcinogen induced head and neck carcinogenesis." Oral oncology **40**(6): 611-623.

Stigler, S. (2008). "Fisher and the 5% level." Chance **21**(4): 12-12.

Thomas, D., J. Matthews, V. Patel, S. Game and S. Prime (1995). "Inflammatory cell infiltrate associated with primary and transplanted tumours in an inbred model of oral carcinogenesis." *Journal of oral pathology & medicine* **24**(1): 23-31.

Urdan, T. C. (2010). Statistics in plain English, Taylor & Francis US.

Viswanath, D. (2004). "The fractal property of the Lorenz attractor." *Physica D: Nonlinear Phenomena* **190**(1-2): 115-128.

Williams, B. (1995). Trading chaos: applying expert techniques to maximize your profits, Wiley.

Yuen, A. P. W., W. I. Wei, Y. M. Wong and K. C. Tang (1997). "Elective neck dissection versus observation in the treatment of early oral tongue carcinoma." *Head & neck* **19**(7): 583-588.

APPENDIX

UNIVERSITY OF ILLINOIS AT CHICAGO

Animal Care (ACC) and Institutional Biosafety Committees (IBC) (MC 672)
Office for the Protection of Research Subjects
Office of the Vice Chancellor for Research
201 Administrative Office Building
1737 West Polk Street
Chicago, Illinois 60612-7227

September 26, 2005

Joel Schwartz
Oral Medicine & Diagnostic Sciences
M/C 838

Dear Dr. Schwartz:

The modifications requested in modification *04-259-01* pertaining to your approved protocol indicated below have been reviewed in accordance with the Animal Care Policies of the University of Illinois at Chicago and approved on *September 26, 2005*.

Title of Application: Tobacco Carcinogen Induced Oral Cancer

ACC Number: 04-259

Modification Number: 04-259-01

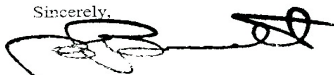
Nature of Modification: *Addition of Personnel: Francis Tan and Weiqing Zhang are approved for painting of carcinogens on tongue of hamster. Additional training will be required if they will assist in assessment of animals (health and humane endpoints).*

For your information, a copy of the UIC Animal Care Policy on Occupational Health Program for Personnel Caring For and Using Animals is enclosed. Please refer to it for your responsibilities and procedures to be followed.

This institution has Animal Welfare Assurance Number A3460.01 on file with the Office of Laboratory Animal Welfare, NIH. Please transmit this letter of acceptable verification of modification of your research protocol to your sponsor.

The records of the Animal Care Committee will be revised to reflect these changes. Thank you for complying with the Animal Care Policies and Procedures of UIC.

Sincerely,



B. Taylor Bennett, DVM, PhD
Chair, Animal Care Committee

BTB/mbb
cc: BRL, ACC File

UIC

Phone (312) 996-7427 • Fax (312) 996-9008

VITA

NAME: Yajur Parikh

EDUCATION: B.S., Computer Engineering, University of Illinois at Urbana-Champaign, 2003
M.S., Bioengineering, University of Illinois at Chicago, 2014

PROJECTS: UIC Bioengineering Student Journal, Reviewer 2010-2011
Engineering World Health, Projects That Matter 2010-2011

INDUSTRY
EXPERIENCE: Motorola 2000-2009
- Summer Intern 2000, 2001, 2002
- Software Engineer 2003-2008
- Senior Software Engineer 2008-2009
HP Software 2011-2014
- Senior Support Solutions Engineer

PROFESSIONAL
MEMBERSHIP: Association of Computing Machinery (ACM)
Institute of Electrical and Electronics Engineers (IEEE)

AWARDS: Six Sigma Quality IQ – Yellow Belt
Motorola BRAVO Award – Nov 2007 – For overseeing and achieving compliance efforts for 802.16e Corrigendum 2 standard
Motorola BRAVO Award – Jun 2008 – For achieving WiMAX Forum Wave2 certification